Transport in transverse magnetic fields in resonant tunneling structures

A. Zaslavsky, Yuan P. Li, D. C. Tsui, M. Santos, and M. Shayegan
Department of Electrical Engineering, Princeton University, Princeton, New Jersey 08544
(Received 26 February 1990)

We report measurements on the magnetotunneling characteristics of a high-quality bistable double-barrier resonant tunneling device in magnetic fields transverse to the tunneling direction. The transverse magnetic field $B_\perp$ causes complex, nonmonotonic shifts in the position of the resonant current peak in the $I(V)$ curve. The resonant peak is also strongly broadened by $B_\perp$, and the peak current is suppressed. The intrinsic bistability of the device is quenched for $B_\perp > 5$ T. We explain these effects by invoking the magnetic-field-induced change in transverse momentum Δk as electrons tunnel into the well. The change Δk alters both the tunneling supply function and the tunneling probability for a given alignment of the resonant subband and the emitter electrode. Self-consistent calculations based on this model reproduce the complex behavior of resonant peak position and explain the experimentally observed magnetic-field effects.

INTRODUCTION

Magnetotunneling measurements on double-barrier resonant tunneling structures (DBRTS) provide an effective means of studying the details of charge transport in these physically interesting and potentially useful devices. The two standard experimental geometries for these measurements involve orienting the B field either parallel or transverse to the tunneling current. Magnetotunneling in a parallel field has been studied by a number of authors,[1-5] who have observed regular field-induced features or steps in the $I(V)$ curve. In a parallel field, $B_\parallel$, the tunneling Hamiltonian is separable and transport along the tunneling direction is independent of transverse momentum. The effect of $B_\parallel$ on the densities of states in both the three-dimensional emitter and the two-dimensional well, as well as on the energy and transverse-momentum conservation rules of resonant tunneling, can be clearly identified. Since in a $B_\parallel$ field resonant tunneling into the well conserves Landau-level index, the observed magnetotunneling steps can be clearly associated with the alignment of Landau levels in the emitter and the well.[1,2]

In a transverse field, $B_\perp$, the situation is more complex, as the confinement by the magnetic field mixes with the heterostructure double-barrier potential in the tunneling direction and transport along the tunneling direction no longer conserves all the transverse-momentum components. For this reason the magnetotunneling data in a transverse field have been more difficult to interpret. To date most studies have noted the shift of the resonant peak caused by the transverse field, which has been qualitatively explained by the $B_\perp$ field-induced change Δk in the transverse momentum as the electron tunnels in and out of the well[6-8] and by the field-induced suppression of the tunneling current (originally investigated in single-barrier structures by Guéret *et al.*[9]). Also, when the DBRTS well is wide compared to the magnetic length, the electronic states far from the barriers have energies determined by the magnetic field alone, while states near the interfaces execute well-defined skipping orbits. Magnetotunneling features due to tunneling into these skipping orbits has been observed by several authors in wide-well DBRTS (Ref. 10) and single-barrier structures.[11]

In our DBRTS, the well is sufficiently narrow to suppress skipping orbits and the experimental $I(V,B_\perp)$ curve does not exhibit any discernible features on the energy scale $\hbar\omega_c$ characteristic of Landau quantization (where $\omega_c \equiv eB_\perp/m^*$ is the cyclotron frequency). Instead we observe field-induced shifts in the peak position V_p of the reverse bias $I(V)$ curve that do not obey a simple B^2 dependence predicted by some authors,[8,12] and significant broadening of the entire resonant $I(V)$ peak. Furthermore, the intrinsic bistability[13] in the forward bias $I(V)$ curve of our DBRTS is reduced by the $B_\perp$ field and quenched entirely for $B_\perp > 5$ T. We explain the field-induced effects in the $I(V,B_\perp)$ curves by calculating the supply function of electrons tunneling into the well for different values of $B_\perp$ and then self-consistently computing the reverse-bias $I(V,B_\perp)$ curves. The resulting $I(V,B_\perp)$ curves adequately reproduce the experimentally observed magnetic field effects in the reverse-bias $I(V,B_\perp)$ characteristic of our DBRTS device. We also propose that the same mechanisms can explain the magnetic quenching of the intrinsic bistability in the forward-bias $I(V,B_\perp)$ characteristic.

EXPERIMENT AND DATA

Our magnetotunneling measurements were performed at 4.2 K in $B_\perp$ fields up to 9.0 T. The details of the molecular-beam epitaxy (MBE)-grown DBRTS structure have already been published elsewhere;[4] for the purposes of this report it suffices to note that the GaAs well is 56 Å wide [well below the magnetic length $L_B = (265/B^{1/2})$ Å, with B in Tesla, even at the highest $B_\perp$ in our experiment], while the asymmetric $Al_xGa_{1-x}As$ barriers are 85

Å wide and have Al mole fractions of $x=0.4$ and $x=0.5$. As discussed elsewhere, the asymmetry of the barriers enhances dynamic charge buildup in the well in the forward-bias polarity (when the higher barrier serves as the collector barrier) leading to a large intrinsic bistability region.[14] The device area was approximately 12×12 μm^2.

The reverse-bias $I(V,B_\perp)$ characteristics of the device for several $B_\perp$ values are plotted in Fig. 1. At $B_\perp=0$ the current begins to rise at the threshold $V_t\approx165$ mV, peaks at 0.196 μA at $V_p=234$ mV, and decreases to the valley region where one also finds the phonon-assisted tunneling replica peak.[15] The overall peak-to-valley ratio is better than 25:1, indicating the high quality and homogeneity of the DBRTS structure. Since in this bias polarity there is very little charge storage in the well, the reverse bias $I(V,B_\perp)$ characteristics are independent of the voltage sweep direction—no intrinsic bistability is observed for any value of $B_\perp$.

When the reverse-bias $I(V,B_\perp)$ is measured at increasing values of $B_\perp$, the line shape of the resonant peak undergoes marked field-dependent modifications. While the threshold voltage remains nearly constant for the entire range of $B_\perp$ (a small shift in V_t towards higher bias is seen for $B_\perp=9$ T), the magnetic field induces sizable shifts in the peak voltage V_p. The behavior of V_p at low magnetic fields is plotted in the inset of Fig. 1: V_p first shifts slightly but unmistakably towards lower bias and then reverses its course. At high $B_\perp$ the voltage peak shifts strongly towards higher bias, eventually reaching $V_p=285$ mV at $B=9.0$ T. The peak current I_p falls off rapidly with $B_\perp$: even a small field of $B_\perp=1.0$ T causes a 10% reduction in I_p, while at $B_\perp=9.0$ T, I_p has been reduced by more than a factor of 2 to 0.086 μA. At the same time the resonant peak becomes much broader, keeping the total integrated current nearly constant. This broadening subsumes the phonon-assisted replica peak, which is no longer visible for $B_\perp\geq4.0$ T.

The forward-bias $I(V,B_\perp)$ characteristics of the device for several values of $B_\perp$ are plotted in Fig. 2. In the zero-field characteristic with the bias ramped up, the current begins to rise at $V_t\approx170$ mV, reaches the peak of 1.32 μA at $V_p=401$ mV, and then drops sharply to the valley region (the current begins to rise again due to tunneling through the second subband near 700 mV; the second peak occurs at $V=1.85$ V and $I=200$ μA). The valley region exhibits a replica peak due to phonon-assisted tunneling. When the voltage is ramped down, the device switches back to the high-current state at $V=357$ mV, producing a bistable region of nearly 45 mV.

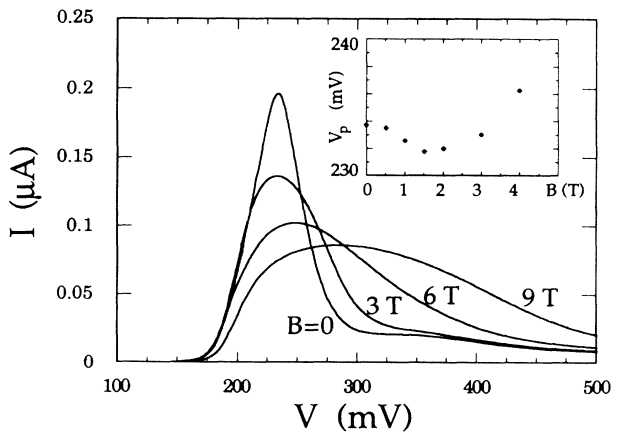

FIG. 1. Reverse-bias $I(V,B_\perp)$ curves at $T=4.2$ K at transverse $B_\perp=0$, 3.0, 6.0, and 9.0 T. Inset shows peak voltage V_p as a function of $B_\perp$ for $0\leq B_\perp\leq4$ T.

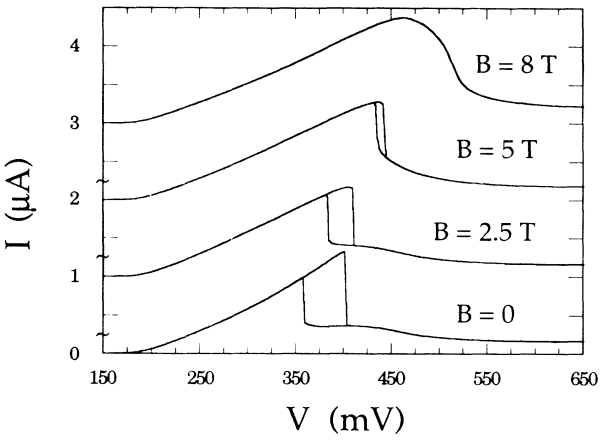

FIG. 2. Forward-bias $I(V,B_\perp)$ curves at transverse $B_\perp=0$, 2.5, 5.0, and 8.0 T. The curves are displaced vertically by 1.0 μA for clarity. The bistability is completely quenched at $B_\perp=6.0$ T.

In the forward-bias polarity at low $B_\perp$, the current peak position V_p, albeit reproducible from measurement to measurement, does not reflect an unambiguous physical quantity, as it is determined by the discontinuous switching of the device from a high- to a low-current state.[13] At higher values of $B_\perp$, where V_p falls in the continuous region of the $I(V)$ curve, the forward-bias $I(V,B_\perp)$ exhibits a pronounced shift of V_p towards higher bias, reaching $V_p=470$ mV at $B_\perp=9.0$ T, while V_t once again remains nearly constant for the entire range of $0\leq B_\perp\leq9$ T. The transverse field broadens the $I(V,B_\perp)$ line shape strongly, rounding the sharp current peak and leading to the progressive narrowing of the bistable region. At fields above 5 T, the intrinsic bistability becomes completely quenched, and $I(V,B_\perp)$ starts reverting to the more symmetrical line shape, similar to the reverse-bias $I(V,B_\perp)$. The broadening line shape subsumes the phonon-assisted replica peak for $B_\perp>3$ T. Unlike the reverse bias, the behavior of the peak current in the forward-bias $I(V,B_\perp)$ does not follow any monotonic dependence on $B_\perp$. While I_p falls with $B_\perp$ at low fields ($B_\perp<5$ T), this process saturates at higher $B_\perp$, and I_p actually increases in the $B_\perp>7$ T range.

It should also be noted that the $B_\perp$ field does not induce any discernible magnetotunneling features on the $\hbar\omega_c$ scale in either the $I(V,B_\perp)$ curve or the conductance dI/dV. In a $B_\parallel$ field, on the other hand, current steps associated with Landau quantization of the density of states in the emitter and well of the DBRTS are clearly observ-

able.[4] The absence of such features in the $I(V,B_\perp)$ curves of our DBRTS device is due to the narrow well that prevents Landau quantization in the well for all transverse fields employed in the experiment. This point will be addressed in more detail in the following discussion of the experimental results.

DISCUSSION

In the absence of a magnetic field, the sequential tunneling model[16] has successfully addressed the fundamental aspects of charge transport through DBRTS devices. In this model the $I(V)$ curve is determined by selection rules that require energy and transverse-momentum conservation for electrons tunneling from the three-dimensional emitter into a two-dimensional resonant subband in the well. These selection rules, in turn, determine the number of electrons $N(\Delta E)$ that can tunnel elastically into the well for a given energy separation of the resonant subband E_0 and the Fermi energy E_F of the electron distribution in the emitter [see Fig. 3(a)]. The current through the device is to the first order proportional to the tunneling supply function $N(\Delta E)$ multiplied by the appropriate transmission coefficient (usually calculated in the Wentzel-Kramers-Brillouin (WKB) approximation). Finally, the energy alignment of the emitter and the resonant subband can be self-consistently related to the total potential distribution over the device,[2] yielding the theoretical $I(V)$ curve.

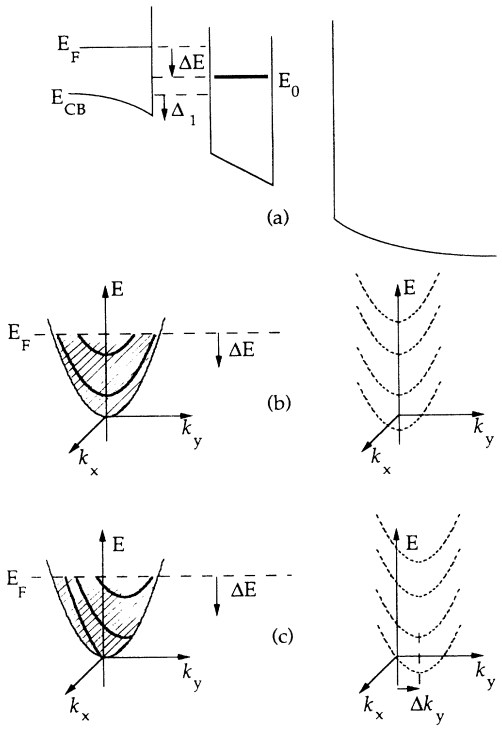

FIG. 3. (a) Energy alignment of the emitter and the resonant subband E_0 in the elastic tunneling regime: $\Delta E \equiv E_F - E_0$ is the energy separation between emitter E_F and E_0; Δ_1 is the energy depth of the accumulation layer; the zero of energy is taken to coincide with the bottom of the conduction band E_{CB} in the emitter. (b) Distribution in the (E,k_x,k_y) energy-momentum space of the occupied emitter electron states (shaded) on the left and the available resonant subband states (dashed lines) on the right at four different values of ΔE for $\Delta k_y = 0$. States that can tunnel elastically are on the boldface sections through the emitter states on the left. (c) The same as in (b), but for $\Delta k_y = 0.4 k_F$ ($B_\perp \approx 3$ T).

A particularly useful feature of the sequential tunneling model is that it can be easily extended to account for magnetic field effects. Earlier we have extended the model to include parallel field magnetotunneling by examining the effect of $B_\parallel$ on the tunneling supply function because of Landau quantization in the emitter and the two-dimensional subband in the well.[4] The $B_\parallel$ features in the supply function combined with the energy and Landau index conservation (which in a $B_\parallel$ field is equivalent to conservation of transverse momentum) during tunneling proved sufficient to explain the experimentally observed parallel field magnetotunneling effects. We shall now extend the sequential tunneling model to incorporate the $B_\perp$ field and thus explain our experimental results. An alternative approach, involving the transfer Hamiltonian formalism,[17–19] has been proposed by Helm *et al.*[10] to explain their data on $B_\perp$-induced shifts of the resonant peaks in the $I(V)$ characteristics of a DBRTS structure with a wide well. However, the sequential tunneling model appears more intuitive, as it permits a simple geometrical evaluation of the effects of $B_\perp$ on the supply function and the tunneling probability for a given bias configuration.

In the absence of scattering, the three-dimensional emitter states would be quantized into Landau cylinders and the density of states would exhibit Landau peaks separated by $\hbar\omega_c$, but because of heavy doping these peaks are strongly broadened. In the undoped well the transverse field $B_\perp$ also does not lead to Landau quantization because the well is too narrow to accommodate the cyclotron orbit for any of the fields in our experiment. The energy quantization in the tunneling direction is still determined by the double-barrier-potential $V(z)$ and $B_\perp$ can be treated as a weak perturbation that contributes a small diamagnetic shift.[20] Accordingly, we find that to first order the density of states in the well is not affected by $B_\perp$ and hence we do not expect to observe any strong magnetotunneling features on the $\hbar\omega_c$ scale in the $I(V,B_\perp)$ characteristics. The main effect of $B_\perp$ on the $I(V)$ curve will arise from the $B_\perp$-induced change in the conservation of transverse momentum.[6–8] Taking the tunneling direction to lie along the z axis, $\mathbf{B}_\perp \| \mathbf{x}$, and working in the Landau gauge, $\mathbf{A} = (0, -B_\perp z, 0)$, one finds that an electronic state in the emitter characterized by the quantum numbers (E,k_x,k_y) can tunnel elastically into a well state with quantum numbers $(E,k_x,k_y-\Delta k_y)$, where E is the energy with respect to some common origin and $\Delta k_y = eB_\perp \langle z \rangle / \hbar$, with $\langle z \rangle$ being the distance along the z axis traversed in the course of tunneling through the emitter barrier.

The above-described selection rules for elastic tunneling in a transverse field, combined with the known material parameters of the DBRTS and a self-consistent

treatment of the potential distribution over the device,[2] make it possible to calculate numerically the $I(V)$ curve of a DBRTS device placed in a $B_\perp$ field. Before presenting the calculation that adequately reproduces the transverse magnetic field effects in our device under reverse bias, we shall present an intuitive geometrical model which provides a simple qualitative interpretation of the observed magnetic effects. The model is essentially summarized in Fig. 3. First consider the case of $B_\perp=0$. In the resonant tunneling regime, where the external bias V aligns the resonant subband with occupied states in the emitter and causes the tunneling current to flow, the band diagram of the device is shown in Fig. 3(a) where we have defined $\Delta E \equiv E_F - E_0$ as the energy separation between the Fermi energy in the emitter and the quantized resonant subband energy in the well (in our sign convention ΔE increases as more bias is applied and E_0 drops lower in energy with respect to the emitter). At low temperatures the electronic states in the three-dimensional emitter occupy a sphere of radius k_F in momentum space, where k_F is the Fermi wave vector. The occupied emitter states can be graphically represented in (E,k_x,k_y) space[21] as a solid made up of a collection of paraboloids $E(E_z)=E_z+\hbar^2(k_x^2+k_y^2)/2m^*$, shown on the left in Fig. 3(b). The energy axis intercepts $E_z=\hbar^2k_z^2/2m^*$ of these paraboloids range from 0 to E_F for all the allowed values of k_z. The states in the well all lie on a single paraboloid $E=E_0(V)+\hbar^2(k_x^2+k_y^2)/2m^*$, where E_0 can be shifted with respect to the emitter by the applied bias V. These states are shown on the right in Fig. 3(b) for four different values of applied bias (corresponding to four values of E_0). At $V=0$ the subband E_0 lies above emitter E_F (i.e., ΔE is negative), the occupied states in the emitter do not overlap with the available states in the well, and no current can flow. As the applied bias is increased, the resonant subband is moved below the emitter E_F. From the conservation of energy and transverse momentum, it then follows that the emitter states which can tunnel elastically at some value of ΔE in the $0<\Delta E\le E_F$ range all lie on the parabola with $E_z=E_F-\Delta E$, drawn in boldface on the left in Fig. 3(b) for two values of ΔE in the tunneling regime. These states make up the zero-field tunneling supply function $N(\Delta E,\Delta k_y=0)$ which is trivially evaluated as $N(\Delta E,\Delta k_y=0)=m^*\Delta E/\pi\hbar^2$.[4,16] If more bias is applied, ΔE increases and, as long as $\Delta E\le E_F$, $N(\Delta E,\Delta k_y=0)$ increases linearly with ΔE. Once the subband E_0 drops below the bottom of the conduction band (i.e., $\Delta E>E_F$), however, energy and momentum conservation can no longer be satisfied [the paraboloids of the emitter and the well have no points in common, see Fig. 3(b)], the supply function drops to zero, and no resonant current can flow. Thus, for $B_\perp=0$, the picture is identical to the original geometrical construction proposed by Luryi[16] to describe sequential tunneling.

Now consider the case of nonzero $B_\perp$. Neglecting the weak Landau quantization in the emitter, the electronic states in the emitter and the well can be treated analogously to the $B_\perp=0$ case, with the crucial difference that when $B_\perp\neq0$, an emitter state (E,k_x,k_y) can now tunnel elastically into the resonant subband state $(E,k_x,k_y-\Delta k_y)$, with $\Delta k_y=eB_\perp\langle z\rangle/\hbar$. Therefore, the state in the emitter that can tunnel elastically into the well at a given ΔE lies on a displaced paraboloid:

$$E=(E_F-\Delta E)+\hbar^2[k_x^2+(k_y-\Delta k_y)^2]/2m^* . \quad (1)$$

This situation is illustrated in Fig. 3(c) for the same values of E_0 as in Fig. 3(b). Once again, the emitter states which can tunnel elastically into the well are shown in boldface on the left. As before, for $\Delta E<0$ no current can flow. When the resonant subband E_0 drops below the emitter E_F, some emitter states will be able to tunnel elastically, but $N(\Delta E,\Delta k_y)$ will differ from $N(\Delta E,\Delta k_y=0)$ once $\Delta E>E_F-\hbar^2\Delta k_y^2/2m^*$. Clearly, the supply function no longer falls to zero when the subband E_0 drops below the bottom of the conduction band. It is thus immediately obvious that a nonzero $B_\perp$ will broaden the supply function and cause it to acquire a high-energy tail for $\Delta E>E_F$. Since the $\langle z\rangle$ factor in $\Delta k_y=eB_\perp\langle z\rangle/\hbar$ is largely independent of ΔE (in fact, $\langle z\rangle$ can be taken as the mean distance between the z coordinates of the peaks in the electron wave functions in the accumulation layer and the well, hence $\langle z\rangle$ should increase slightly with applied bias), the calculation of $N(\Delta E,\Delta k_y)$ presents no difficulty. In Fig. 4 we plot $N(\Delta E,\Delta k_y)$ for $\Delta k_y=0$, 0.4, 0.8, and 1.2 in units of k_F (for $E_F=20$ meV and $\langle z\rangle\approx160$ Å, appropriate to our DBRTS, these values of Δk_y approximately correspond to $B_\perp=0$, 3, 6, and 9 T). Note that near $\Delta E=0$, $N(\Delta E,\Delta k_y)\sim\Delta E$ as long as $\Delta k_y\le k_F$, and hence the threshold bias V_t should not shift with $B_\perp$ as long as $B_\perp\le7.5$ T, in agreement with the data in Fig. 1.

It is important to note, however, that while the $I(V,B_\perp)$ curve is certainly determined by $N(\Delta E,\Delta k_y)$, no reliable information on the $I(V,B_\perp)$ line shape can be extracted from $N(\Delta E,\Delta k_y)$ alone. For example, although some authors have attempted to fit the shift of the peak V_p to a $B_\perp^2$ dependence,[8,11] it is clear from Fig. 1 that while V_p generally shifts towards higher bias as $B_\perp$ is increased, the actual behavior of V_p is complicated. In particular, we find experimentally that V_p initially decreases

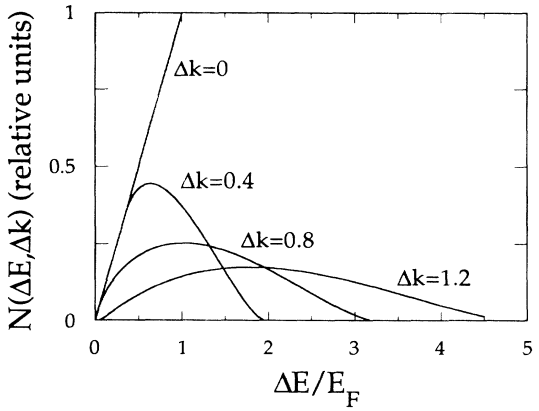

FIG. 4. Supply function $N(\Delta E,\Delta k_y)$ for $\Delta k_y=0$, 0.4, 0.8, and 1.2 in units of k_F (corresponding to $B_\perp\approx0$, 3, 6, and 9 T).

as $B_\perp$ is increased from 0 to 2.0 T (see inset of Fig. 1). In order to properly analyze the $I(V,B_\perp)$ line shape, one must self-consistently calculate the current, taking into account the potential distribution over the device. If one assumes that all of the electronic states in the well that satisfy the tunneling selection rules are actually available (in other words, if charge buildup in the well is negligible, which is the case for the reverse-bias polarity in our DBRTS), the current density through the device at a given ΔE and $B_\perp$ can be approximated by[13]

$$J(\Delta E,B_\perp)\simeq(e/2\pi\hbar)N(\Delta E,\Delta k_y)\bar{T}_e(E_F+\Delta_1-\Delta E)\ , \quad (2)$$

where $\bar{T}_e$ is the average transmission coefficient of the emitter barrier and the other quantities are defined in Fig. 3(a). In the WKB approximation, T_e depends on the energy E_z of the emitter electrons in the tunneling direction only. If $B_\perp=0$, the electrons that satisfy the conservation rules for a given ΔE all have the same E_z [see Fig. 3(b)] and consequently tunnel with the same transmission coefficient T_e. Furthermore, as ΔE increases, these electrons tunnel through a higher barrier [see Fig. 3(a)]. Thus, when $B_\perp=0$, $J(\Delta E,0)$ is the product of a linearly increasing supply function, $N(\Delta E,0)\sim\Delta E$, and a decreasing transmission coefficient T_e. The peak current I_p need not coincide with the peak in the supply function and the theoretical $I(V)$ curve must be calculated self-consistently.

The presence of a nonzero $B_\perp$ can affect the current density in two ways. First, the $B_\perp$ field can reduce the transmission coefficient T_e by altering the "trajectory" of the tunneling electron and increasing the effective barrier. This effect has been reported in tunneling through a single barrier,[9,12] but the measured reduction was almost negligible in magnetic fields below 4.0 T in the case of a 168-Å $Al_{0.35}Ga_{0.65}As$ barrier.[12] Our data, on the other hand, exhibit a significant drop in the current at low $B_\perp$. The second effect, which we believe is the dominant one, arises because of the energy and canonical momentum conservation in the presence of $B_\perp$, which couples emitter states with quantum numbers (E,k_x,k_y) to the states in the well with numbers $(E,k_x,k_y-\Delta k_y)$ and thus changes the supply function as shown in Fig. 3(d). Furthermore, in contrast to the $B_\perp=0$ ($\Delta k_y=0$) situation, the tunneling states with different k_y now have different values of E_z, and the average transmission coefficient $\bar{T}_e$ must be numerically evaluated as an integral over k_y weighted by the values of $N(\Delta E,\Delta k_y)$.

In order to verify that the above-discussed model can really simulate the observed $B_\perp$ effects in the $I(V)$ curve of our DBRTS, we have carried out a self-consistent numerical calculation of $I(V,B_\perp)$ for different values of $B_\perp$. The self-consistent potential distribution over the device was computed according to the system of equations in Ref. 2; the actual numerical procedure was described in an earlier paper.[4] Since the calculation of $I(V,B_\perp)$ requires an additional integration of the transmission coefficient T_e over k_y and is consequently much more cumbersome than the calculation of $I(V,B_\parallel)$,[4] we have concentrated on the reverse-bias polarity, where the effects of space charge buildup in the well are small and easily calculated. As is usually the case when the WKB approximation for the transmission coefficients is used, the calculated current densities disagree with experimental data—in our case they are too large by nearly an order of magnitude. Once the calculated $I(V,B_\perp=0)$ peak current is normalized to the measured I_p, however, the calculated $I(V,B_\perp)$ line shapes reproduce the experimentally observed $B_\perp$ field effects, including the resonant peak broadening, the behavior of the threshold voltage V_t, the appearance of a long tail at the high-bias side of the peak, the reduction in I_p as $B_\perp$ increases, and the field-induced shifts in V_p (the calculated V_p first moves towards lower bias and then shifts out). The results are shown in Fig. 5 for $\Delta k_y=0$, 0.4, 0.8, and 1.2 in units of k_F (corresponding to $B_\perp\approx0$, 3, 6, and 9 T, respectively) for the same material parameters previously used to calculate $I(V,B_\parallel)$ (Ref. 4) (barriers of 320 and 433 meV, electrode doping of $\sim2\times10^{17}$ cm^{-3}, and spacer layers of ~50 Å outside the barriers). The unrealistically sharp turn on of the current at V_t is due to the assumption of zero temperature and neglect of band tailing in the calculation. Given these and other limitations of the calculation—use of the WKB approximation for the transmission coefficients, neglect of inelastic tunneling and of the contribution by the broadened 2D electron states in the accumulation layer to the supply function, and the assumption of uniform material parameters—the agreement between the experimental data and the calculation is quite good. We note here that in the calculation the mean distance $\langle z\rangle$ traversed by electrons tunneling from the emitter accumulation layer into the well was taken as 160 Å, which is reasonable for our DBRTS parameters.

Finally, let us consider the quenching of the intrinsic bistability in the forward-bias $I(V,B_\perp)$ characteristics of our DBRTS device by fields $B_\perp>5$ T. The forward-bias

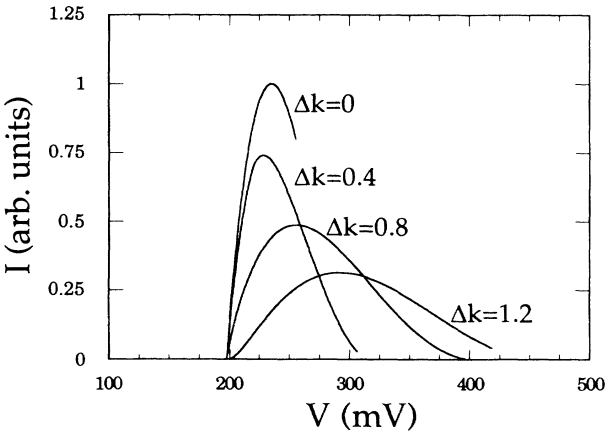

FIG. 5. Calculated reverse-bias $I(V,B_\perp)$ curves for $\Delta k_y=0$, 0.4, 0.8, and 1.2 k_F (corresponding to $B_\perp\approx0$, 3, 6, and 9 T) at zero temperature. The calculated peak of the $B_\perp=0$ current is normalized to the measured reverse-bias peak current (see Fig. 1). Once this is done the other $I(V,B_\perp)$ curves contain no adjustable parameters. The self-consistent calculation and parameters are described in the text.

polarity (wherein the emitter barrier is lower than the collector barrier) maximizes the charge buildup in the well. Given the presence of significant electron density n_w in the well, Eq. (2) for the tunneling current flowing into the well must be multiplied by the additional factor[4]

$$\gamma(\Delta E, n_w) = 1 - \frac{n_w}{(m^* \Delta E / \pi\hbar^2)} , \tag{3}$$

which determines the fraction of the states in the well that are not occupied by n_w at a given band alignment ΔE. In steady state, the tunneling current flowing out of the well is given by the equation[2]

$$J = e n_w E_0 T_c / \hbar , \tag{4}$$

where T_c is the transmission coefficient of the collector barrier. The self-consistent calculation of the forward-bias $I(V, B_\perp = 0)$ curve,[4] taking into account the screening effect of n_w on the emitter barrier, indicates that at V_p the densities of electrons stored in the emitter accumulation layer $n_{e,p}$ and the well $n_{w,p}$ are 5×10^{11} and 2.8×10^{11} cm^{-2}, respectively. In the presence of nonzero $B_\perp$ the self-consistent calculation of the forward-bias $I(V, B_\perp)$ becomes extremely cumbersome, but a rough estimate of $B_\perp$ required to quench the intrinsic bistability can be obtained from the following considerations.

The mechanism responsible for the switching of the device from the high- to the low-current state is the discharging of n_w. Once the peak current I_p and $n_{w,p}$ are reached at V_p, a small increase in applied bias ΔV cannot supply more current into the well because the supply function has reached its maximum. At the same time, the current flowing out of the well does increase with ΔV and the well begins to discharge. To maintain a constant total potential drop over the DBRTS, the external voltage source then supplies more charge to the accumulation layer, which further increases ΔE beyond the maximum in the supply function [see Fig. 3(d)], hence providing positive feedback to the discharge of n_w. If the falloff in the supply function beyond the peak is rapid, a small increase of ΔV will completely discharge the well and switch the device to the low-current state (in the absence of inelastic processes, the valley current would be zero and hence $n_w \to 0$). If we neglect the valley current, let $n_w \to 0$ beyond V_p, and assume that the potential drops in the emitter accumulation and collector depletion layers are, to first order, not affected by the charge redistribution between the well and the emitter (i.e., neglecting the change in electric field outside the barriers), as $n_w \to 0$, we find that to first order $n_e \to n_{e,p} + (n_{w,p}/2)$.[2,22] The resonant subband E_0 then drops (equivalently, ΔE increases) by approximately $e^2(n_{w,p}/2\epsilon)(W_b + W_w/2)$, where ϵ is the permittivity and W_b and W_w are, respectively, the widths of the emitter barrier and the well. At $B_\perp = 0$, we have $n_{w,p} \approx 2.8 \times 10^{11}$ cm^{-2} and ΔE increases by ~ 20 meV as the well discharges. Self-consistent calculations[2,4] show that the forward-bias V_p corresponds to $\Delta E \approx E_F$ and hence an increase in ΔE by ~ 20 meV will move the system into the region where the supply function is zero (see Fig. 4). As $B_\perp$ increases, however, the supply function acquires a large tail beyond $\Delta E = E_F$, as shown in Fig. 4. Whereas at $B_\perp = 3.0$ T ($\Delta k_y \approx 0.4\ k_F$) a shift of ~ 20 meV beyond the peak will decrease $N(\Delta E, \Delta k_y = 0.4)$ by an order of magnitude, at $B_\perp = 6.0$ T ($\Delta k_y \approx 0.8\ k_F$) such a shift will only slightly decrease $N(\Delta E, \Delta k_y = 0.8)$, and no abrupt switching to a low-current state should occur. Thus, by examining the supply functions corresponding to different $B_\perp$ we find that, for our DBRTS parameters, the model predicts a quenching of intrinsic bistability between $B_\perp = 3$ T and $B_\perp = 6$ T, which agrees with the experimental results.

In conclusion, we have studied the transverse magnetic field effects in the $I(V, B_\perp)$ characteristics of a high-quality DBRTS device. We found that a transverse field $B_\perp$ causes marked changes in the line shape of the $I(V)$ curve: while the threshold bias is nearly unchanged, the current peak is suppressed and broadened, and the peak position shifts in a complex fashion. We have interpreted our results by addressing the effects of the transverse field on the tunneling supply function and the tunneling transmission probability that together determine the elastic tunneling current. We have presented an intuitive geometrical approach that sheds light on the tunneling selection rules that determine the magnetotunneling current, and have supported our interpretation with numerical simulations of the reverse-bias $I(V, B_\perp)$ curve for different values of $B_\perp$. Finally, we have given a qualitative account of how these same mechanisms can lead to the quenching of intrinsic bistability in the forward-bias polarity, where numerical simulation of the $I(V, B_\perp)$ curve becomes prohibitively complex. A possible subject of future study could be measurements in very high magnetic fields ($B_\perp > 20$ T) that would make the Landau quantization comparable to the subband quantization by the double-barrier potential and lead to a transition from a narrow- to a wide-well behavior.

ACKNOWLEDGMENTS

The authors gratefully acknowledge numerous helpful discussions with Dr. M. Frei and technical assistance in the MBE sample growth by T. Sajoto. This work has been supported by the Army Research Office.

[1] E. E. Mendez, L. Esaki, and W. I. Wang, Phys. Rev. B **33**, 2893 (1986).

[2] V. J. Goldman, D. C. Tsui, and J. E. Cunningham, Phys. Rev. B **35**, 9387 (1987).

[3] C. A. Payling, E. S. Alves, L. Eaves, T. J. Foster, M. Henini, O. H. Hughes, P. E. Simmonds, J. C. Portal, G. Hill, and M. A. Pate, J. Phys. (Paris) Colloq. **48**, C5-289 (1987); M. L. Leadbeater, E. S. Alves, L. Eaves, M. Henini, O. H. Hughes, A. Celeste, J. C. Portal, G. Hill, and A. Pate, Phys. Rev. B **39**, 3438 (1989).

[4] A. Zaslavsky, D. C. Tsui, M. Santos, and M. Shayegan, Phys. Rev. B **40**, 9829 (1989).

[5]S. Ben Amor, K. P. Martin, J. J. L. Rascol, R. J. Higgins, R. C. Potter, A. A. Lakhani, and H. Hier, Appl. Phys. Lett. **54**, 1908 (1989).

[6]R. A. Davies, D. J. Newson, T. G. Powell, M. J. Kelly, and H. W. Myron, Semicond. Sci. Technol. **2**, 61 (1987).

[7]M. L. Leadbeater, L. Eaves, P. E. Simmonds, G. A. Toombs, F. W. Sheard, P. A. Claxton, G. Hill, and M. A. Pate, Solid State Electron. **31**, 707 (1988).

[8]P. England, J. R. Hayes, M. Helm, J. P. Harbison, L. T. Florez, and S. J. Allen, Jr., Appl. Phys. Lett. **54**, 1469 (1989).

[9]P. Guéret, A. Baratoff, and E. Marclay, Europhys. Lett. **3**, 367 (1987).

[10]M. Helm, F. M. Peeters, P. England, J. R. Hayes, and E. Colas, Phys. Rev. B **39**, 3427 (1989).

[11]B. R. Snell, K. S. Chan, F. W. Sheard, L. Eaves, G. A. Toombs, D. K. Maude, J. C. Portal, S. J. Bass, P. Claxton, G. Hill, and M. A. Pate, Phys. Rev. Lett. **59**, 2806 (1987).

[12]L. Eaves, K. W. H. Stevens, and F. W. Sheard, in *The Physics and Fabrication of Microstructures,* edited by M. J. Kelly and C. Weisbuch (Springer-Verlag, New York, 1986), p. 343.

[13]V. J. Goldman, D. C. Tsui, and J. E. Cunningham, Phys. Rev. Lett. **58**, 1256 (1987).

[14]A. Zaslavsky, V. J. Goldman, D. C. Tsui, and J. E. Cunningham, Appl. Phys. Lett. **53**, 1408 (1988).

[15]V. J. Goldman, D. C. Tsui, and J. E. Cunningham, Phys. Rev. B **36**, 7635 (1988).

[16]S. Luryi, Appl. Phys. Lett. **47**, 490 (1985).

[17]M. C. Payne, J. Phys. C **19**, 1145 (1986).

[18]L. Brey, G. Platero, and C. Tejedor, Phys. Rev. B **38**, 9649 (1988).

[19]F. Ancilotto, J. Phys. C **21**, 4657 (1988).

[20]The problem of finding the energy levels in a quantum well in the presence of a transverse magnetic field can be essentially reduced to finding the energy levels of a displaced harmonic oscillator in a box; see R. Vawter, Phys. Rev. **174**, 749 (1968).

[21]A similar construction was first introduced to study magnetotunneling in superlattices by K. K. Choi, B. F. Levine, N. Jarosik, J. Walker, and R. Malik, Phys. Rev. B **38**, 12 362 (1988).

[22]F. W. Sheard and G. A. Toombs, Appl. Phys. Lett. **52**, 1228 (1988).